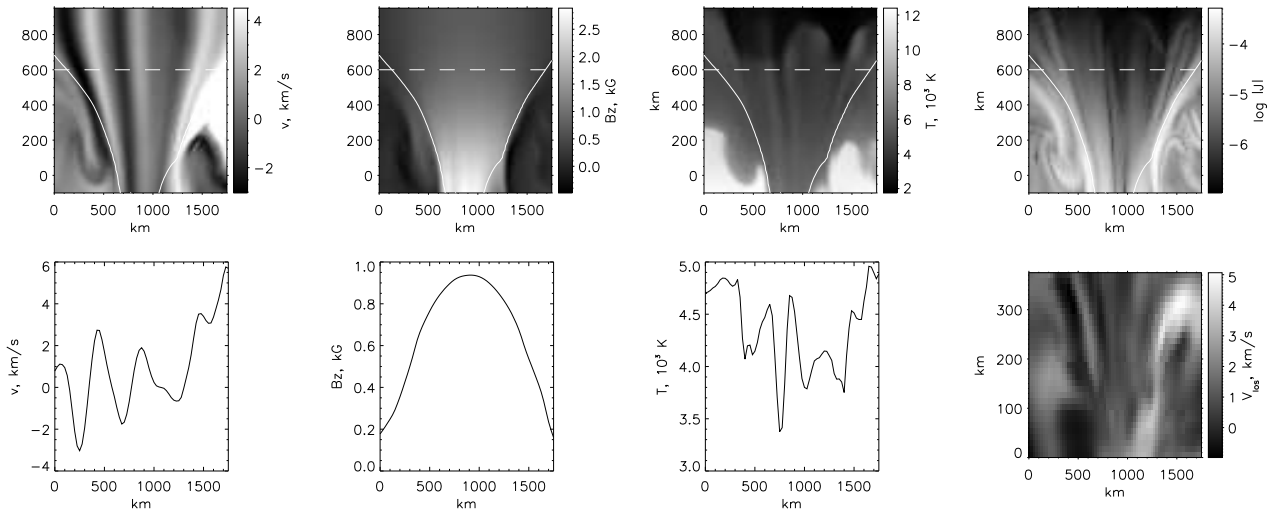

Fig. 2. Magneto-hydrodynamic parameters of a simulated photospheric "vortex" structure, marked by the box in Fig. 1. Top row: the horizontal velocity (the component directed to the observer), the vertical component of magnetic field, the temperature, and the logarithm of the modulus of current density $\mathbf{J} = \nabla \times \mathbf{B}$ vertical cuts through the "vortex". Bottom row: the corresponding cuts of the aforementioned quantities, measured at 600 km above the approximate level of the continuum formation, and the FeI 6302Å absorption line Doppler shift map for the region. Note that the Doppler shift map is rotated counter-clockwise by 90° to align with other quantities in this figure. The contours in the top row bound the region with plasma $\beta < 1$.

the granules facing the observer, and as red-shited regions at those facing away from the observer. At a 60° observational angle (right column), the corrugated optical surface of solar granulation hides the intergranular downflows, while divergent granular flows become significantly more pronounced. However, plenty of small-scale features, nearly co-located with the strong magnetic field regions (second row of the figure), emerging from the intergranular lanes and aligned with the direction of inclination, appear. Notably, no such structures in the continuum intensity images are found. These structures in the COG Doppler shift of FeI 6302.5 Å demonstrate observable presence of small-scale horizontal flows in the magnetised intergranular lanes of the simulation. One of these structures is marked by the box in Fig. 1 and used for further investigation.

The fourth row of Fig. 1 shows Stokes-V area asymmetries, which are calculated by integrating Stokes-V profiles over wavelength and normalising it by the total Stokes-V areas, according to

$$A_V = \frac{\int V d\lambda}{\int |V| d\lambda}. \quad (3)$$

As the figures show, at the solar disk centre (left column), the regions with the largest Stokes-V asymmetry are the boundaries between the magnetised intergranular lanes and the weakly-magnetised granules. This is due to the presence of strong gradients of the line-of-sight velocity and magnetic field components in these regions (Illing et al. 1975; Grossmann-Doerth et al. 1988; Solanki 1989; Khomenko et al. 2005; Shelyag et al. 2007). The situation remains nearly unchanged for 30° inclination (middle row), while the regions with larger asymmetries are more pronounced and occupy larger areas, possibly due to the same mechanism of Stokes-V asymmetry generation. At 60°, however, in a similar manner to the COG Doppler shift discussed above, together with spatially large areas of enhanced asymmetry generated in granular regions, the small-scale elongated structures appear.

A similarity between the horizontal velocity structure in the simulations, FeI 6302.5 Å line Doppler shift and its Stokes-V area asymmetry (Fig. 1) can be demonstrated with Fig. 2. In the top row of the figure, the horizontal velocity component (directed towards the observer), the vertical component of magnetic field, the temperature, and the modulus of current density $\mathbf{J} = \nabla \times \mathbf{B}$ are shown for vertical cuts through the magnetic field concentration marked by the box in Fig. 1. The contours bound the regions with plasma $\beta < 1$. In the bottom row of the figure, the horizontal velocity, the vertical magnetic field and the temperature are shown for a height of 600 km above the approximate level of continuum formation in the magnetic flux tube, marked by 0 height in the top row. The bottom-right panel in the figure is the COG Doppler velocity map of the selected region.

The top-left plot of the figure shows presence of plasma, moving horizontally in opposite directions (towards and away from the observer), within the magnetic field concentration (Shelyag et al. 2011b), where the vertical magnetic field reaches 0.9 kG, as shown in the top and bottom plots in the second column of Fig. 2. The plasma in the intergranular magnetic field concentration experiences some heating (as shown in third column of the figure) due to Ohmic dissipation of currents (Moll et al. 2012) in the magnetic field concentration (top-right plot).

By comparison of the Doppler velocity map (bottom-right panel) and the horizontal velocity field structure (top-left panel) in Fig. 2, a conjecture can be made that

the horizontal velocity motions in the photospheric intergranular magnetic field concentrations manifest themselves as the COG Doppler shifts of FeI 6302.5 Å absorption line and produce Stokes-V asymmetry at large observational angles (see Fig. 1). The asymmetry can be produced by a flow and magnetic field, simultaneously oscillating in the region of the line formation. As suggested by Shelyag et al. (2013), the photospheric magnetic "vortices" are short-lived, oscillatory, transient events, which are manifestations of torsional Alfvén-type oscillations.

4. Degraded images

Finally, we performed the simulated image degradation in a manner approximately representing Hinode Solar Optical Telescope (SOT) observations. The calculated Stokes-I profiles were convolved with Gaussian functions with $\sigma = 0.2''$ for spatial resolution and with $\sigma = 0.0215$ Å for spectral resolution (Tsuneta et al. 2008). After the degradation, the profiles were subjected to the same procedure of COG Doppler shift calculation. No instrumental noise has been added in this modelling. The original (non-degraded) and degraded images are shown in upper and lower panels of Fig. 3. As is evident from comparison of the degraded and original image, the small-scale structures in Doppler velocities completely disappear after the image degradation, while granular structure is clearly visible. This result suggests that higher-resolution observations are needed for the detection of photospheric Alfvén waves. The original resolution of the images was 25 km (~ 0.04 arcsec), which is the planned spatial resolution of the Advanced Technology Solar Telescope (ATST). Thus, future large-aperture instruments will be able to resolve this small-scale photospheric process.

However, it should be noted that the FeI 6302.5 Å line can be not the best choice for Alfvén wave detection. This line is formed in the low to mid photosphere, with the maximum of contribution function located at about 200 km above the continuum formation layer (Sánchez Almeida & Lites 2000; Khomenko & Collados 2007; Vigeesh et al. 2011). Therefore, this line does not track the rich horizontal flow structure in the higher photosphere, as shown in Fig. 2. Including more realistic non-LTE effects in spectral line profile synthesis would lead to even deeper FeI line formation in the photosphere, as demonstrated by Shchukina & Trujillo Bueno (2001). Nevertheless, it is suggested that torsional motions in the photospheric plasma, detected using local correlation tracking in observations, can be related to generation of torsional Alfvén waves (Matsumoto & Kitai 2010).

5. Conclusions

In this paper, we performed spectro-polarimetric diagnostics of a solar photospheric magneto-convection model at three different observation angles. The primary aim for this study was to detect possible observational signatures for horizontal, torsional, Alfvén-type motions in photospheric magnetic flux tubes. Using a photospheric absorption line of iron (FeI 6302.5 Å), we found such signatures in the centre-of-gravity Doppler line shift, as well as in the Stokes-V area asymmetries. As it is shown, the perturbations, introduced in the Stokes profiles by torsional plasma motions in the low plasma-β intergranular magnetic field concentrations, are observed only at high inclination angles. These features are found to be of very small spatial scales, less than the size of intergranular lanes. Aiming to confirm this finding at an observable resolution, we degraded the obtained images in order to mimic properties of Solar Optical Telescope (SOT) onboard the Hinode satellite. As expected, the small-scale features disappeared after degradation. However, as the non-degraded images suggest, it would be possible to detect the Alfvén wave signatures using an instrument with spatial resolution of about 0.04 arcsec. Such spatial resolution is expected to be delivered by ATST, currently under construction.

Another option would be a more appropriate choice of photospheric absorption line. FeI 6302.5 Å is formed deep in the solar photosphere, therefore it is unable to track upper-photospheric regions, where larger-scale torsional motions in the magnetic flux tubes are demonstrated in the simulations, due to expansion of the magnetic flux tubes with height.

Finally, the result, presented in this paper, should be considered as another confirmation of the urgent need for observational instruments with larger apertures and higher resolutions for solar physics research.

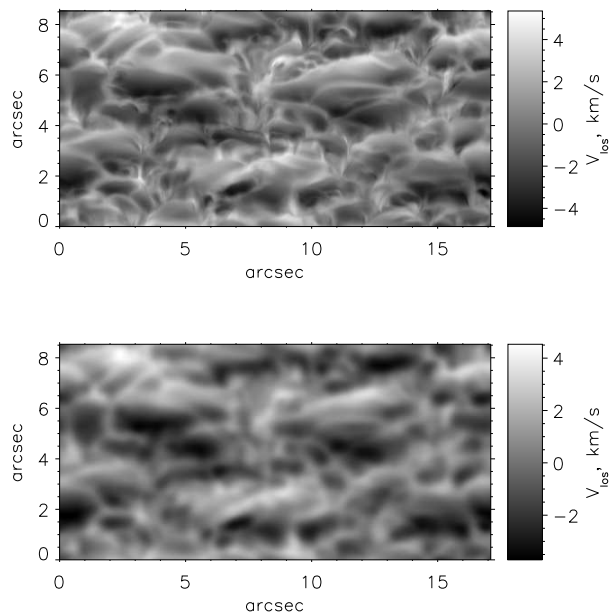

Fig. 3. Original (top) and degraded (bottom) maps of line-of-sight velocities of FeI 6302.5 Å, computed for the simulated photosphere.

6. Acknowledgements

This research was undertaken with the assistance of resources provided at the NCI National Facility systems at the Australian National University, supported by Astronomy Australia Limited, and at the Multimodal Australian ScienceS Imaging and Visualisation Environment (MASSIVE) (www.massive.org.au). The authors also gratefully thank Centre for Astrophysics & Supercomputing of Swinburne University of Technology (Australia) for the computational resources provided. Dr Shelyag is the recipient of an Australian Research Councils Future Fellowship (project number FT120100057). The authors also thank the anonymous referee for a number of useful comments and suggestions which greatly improved the manuscript.

References

Bonet, J. A., Márquez, I., Sánchez Almeida, J., Cabello, I., & Domingo, V. 2008, ApJL, 687, L131
Carlsson, M., Stein, R. F., Nordlund, Å., & Scharmer, G. B. 2004, ApJL, 610, L137
Grossmann-Doerth, U., Schuessler, M., & Solanki, S. K. 1988, A&A, 206, L37
Fujimura, D., & Tsuneta, S. 2009, ApJ, 702, 1443
Illing, R. M. E., Landman, D. A., & Mickey, D. L. 1975, A&A, 41, 183
Irwin, A. W. 2012, Astrophysics Source Code Library, 11002
Jess, D. B., Mathioudakis, M., Erdélyi, R., et al. 2009, Science, 323, 1582
Khomenko, E. V., Shelyag, S., Solanki, S. K., Vögler, A. 2005, A&A, 442, 1059
Khomenko, E., & Collados, M. 2007, ApJ, 659, 1726
Martinez Pillet, V., Lites, B. W., & Skumanich, A. 1997, ApJ, 474, 810
Matsumoto, T., & Kitai, R. 2010, ApJL, 716, L19
Moll, R., Cameron, R. H., & Schüssler, M. 2012, A&A, 541, A68
Morton, R. J., Verth, G., Fedun, V., Shelyag, S., & Erdélyi, R. 2013, ApJ, 768, 17
Panasenco, O., Martin, S. F., & Velli, M. 2014, Sol. Phys., 289, 603
Sánchez Almeida, J., & Lites, B. W. 2000, ApJ, 532, 1215
Shchukina, N., & Trujillo Bueno, J. 2001, ApJ, 550, 970
Shelyag, S., Schüssler, M., Solanki, S. K., Berdyugina, S. V., Vögler, A. 2004, A&A, 427, 335
Shelyag, S., Schüssler, M., Solanki, S. K., Vögler, A. 2007, A&A, 469, 731
Shelyag, S., Keys, P., Mathioudakis, M., & Keenan, F. P. 2011a, A&A, 526, A5
Shelyag, S., Fedun, V., Keenan, F. P., Erdélyi, R., & Mathioudakis, M. 2011b, Annales Geophysicae, 29, 883
Shelyag, S., Mathioudakis, M., & Keenan, F. P. 2012, ApJL, 753, L22
Shelyag, S., Cally, P. S., Reid, A., & Mathioudakis, M. 2013, ApJL, 776, L4
Socas-Navarro, H., Trujillo Bueno, J., & Ruiz Cobo, B. 2000, ApJ, 544, 1141
Socas-Navarro, H. 2011, A&A, 529, A37
Solanki, S. K. 1989, A&A, 224, 225
Tsuneta, S., Ichimoto, K., Katsukawa, Y., et al. 2008, Sol. Phys., 249, 167
Van Doorsselaere, T., Nakariakov, V. M., & Verwichte, E. 2008, ApJL, 676, L73
Vigeesh, G., Steiner, O., & Hasan, S. S. 2011, Sol. Phys., 273, 15
Vögler, A., Shelyag, S., Schüssler, M., et al. 2005, A&A, 429, 335
Wedemeyer-Böhm, S., & Rouppe van der Voort, L. 2009, A&A, 507, L9
Wedemeyer-Böhm, S., Scullion, E., Steiner, O., et al. 2012, Nature, 486, 505